 doi:10.20944/preprints202102.0010.v1

Article

A Comparison of Single-Entry and Multiple-Entry Casing Impingement Manifolds for Active Thermal Tip Clearance Control

Priyanka Dhopade [1,*], Benjamin Kirollos [1], Peter Ireland [1], Leo Lewis [1]

[1] Oxford Thermofluids Institute, Department of Engineering Science, University of Oxford, Oxford, OX20ES, UK.

* Correspondence: priyanka.dhopade@eng.ox.ac.uk

Abstract: In this paper, we investigate the aerothermal performance of active clearance control (ACC) methods that use impingement as a means of enhancing heat transfer. We describe a numerical approach to compare the aerothermal performance of two circumferential impingement manifold supply designs that vary in the number of entry points to the manifold channel. For a 180°-sector, the first design has a single entry point, while the second has two. Both the single-entry and multiple-entry systems analysed in this paper are idealised version of ACC systems in current production engines. Aerothermal performance is quantitatively assessed on the basis of the HTC distribution, driving temperature difference for heat transfer between the jet and casing wall, and total pressure loss within the HPT ACC system. We conclude key advantages and disadvantages of each system based on the impact on engine efficiency, response time, ease of optimisation and implications for weight, cost and complexity of the design.

Keywords: Impingement, heat transfer, manifold, tip clearance, active flow control, gas turbine

1. Introduction

The aviation industry has identified the accelerated development of ACC systems as key to delivering the ACARE Vision 2020 targets of increased efficiency, reduced emissions and increased time-on-wing 1. ACC reduces turbine tip leakage flow, irreversible mixing, diffusion and instabilities, which increases stage efficiency 2 and lengthens engine service life--a considerable advantage given a major engine overhaul can cost upwards of $1M 3. High-pressure turbine (HPT) ACC has been shown to improve net specific fuel consumption (SFC) by 0.7% over non-HPT ACC engines 4, with the potential to increase to > 1% with further optimisation of the HPT ACC system 5. NOx and CO emissions are reduced by 10% and 16%, respectively, with the implementation of HPT ACC on short haul aircraft 6.

A key parameter in the design of HPT and low-pressure turbine (LPT) ACC systems is the relative growth rate of the turbine casing and rotor disk, being an engine-specific function of component thermal masses, core/system aero-thermal fields, fixture locations, and symmetric/asymmetric flight and engine loads 3. Pinch points, i.e. the periods of minimum tip clearance, traditionally occur at take-

Preprints (www.preprints.org) | NOT PEER-REVIEWED | Posted: 1 February 2021 doi:10.20944/preprints202102.0010.v1

off, reacceleration and stop-cock events 7, though some recent production engines pinch at steady cruise due to thermally lighter rotor disks 8.

The vast majority of turbine ACC systems in commercial aero-engines use an active thermal management approach 3. Air that is relatively cheap in terms of cycle efficiency is extracted from the bypass or compressor and impinged against the external side of the turbine casing in order to control turbine casing growth. Depending on the engine and mission specific flight tip clearance profile, thermal response characteristics and operating point, HPT/LPT ACC air is either supplied from the fan duct (e.g. 9), or the compressor (e.g. 4). Turbine ACC systems are typically activated during cruise to reduce passive clearance (e.g. 10), but there is increased effort to develop fast-acting turbine ACC systems (< 5 seconds response time) to accommodate rapid rotor growth during take-off, reacceleration and stop-cock events 6.

1.1 Optimising thermal ACC systems

The optimum active thermal ACC geometry varies from engine to engine, but the over-arching aero-thermal design philosophy for turbine ACC systems is basically the same; namely, to minimise the ACC air flow and time required to deliver the target casing temperature and turbine tip clearance. Setting the target tip clearance is a non-trivial balance between efficiency, reliability, emissions, time-on-wing and complexity, so it is common to break the conjugate optimisation problem into simplified non-conjugate objectives for the ACC system:

i. Maximise the heat transfer coefficient (HTC) enhancement on the external casing generated by the impinging jets, for a given pressure drop within the ACC system
ii. Generate circumferentially and axially uniform HTC for uniform tip clearance
iii. Maximise the temperature difference between the impinging jet and the external side of the casing, to increase the rate of convective cooling for a given HTC.

These principles have driven the latest advances in impingement hole spacing 11, hole shaping 12 and separation distances 10 in ACC manifolds. Overall performance may be further improved by adding model fidelity, e.g. asymmetric clearance effects (affecting the optimum circumferential HTC distribution), the non-linearity between HTC and pressure drop (such that the overall pressure ratio becomes an optimisable parameter), and conductive and radiative heat transfer 13.

Equally important are capex and opex drivers on weight, manufacturability, maintenance, reliability (on and off design), material cost, and size. The entire ACC system from offtake to vent must be considered: thermal expansion joints, support structures, control valves etc. Another, subtler driver in ACC design is the ease with which an architecture can be optimised, because the sensitivity of architecture to perturbations in operating and geometric boundary conditions is a good indication of the potential reliability of the system and influences engine development cost and time-line.

1.2 Impingement manifold supply system

Preprints (www.preprints.org) | NOT PEER-REVIEWED | Posted: 1 February 2021 doi:10.20944/preprints202102.0010.v1

A topic that has not been investigated in the literature--and the focus of this paper--is the optimum method for feeding fan/compressor air into the impingement manifold. There are two main feed architectures that are utilised in current production commercial aero-engines:

1. *Single-entry casing impingement manifolds*. The casing impingement manifold is supplied at a single circumferential location via a collector box. The impingement manifold is either a single 360° annulus or two 180° sectors. Examples of single-entry casing impingement manifolds include the MTU aero-engine shown in Figure **1**, the GE CF6-6 architecture shown in Figure 2 and the engine-scale experiments of Dann et al. 14.

2. *Multiple-entry casing impingement manifolds.* The casing impingement manifold is fed at multiple circumferential locations, typically four, from a secondary ring main, via connectors (also known as transfer boxes). The impingement manifold is split into annular sectors. The ring main is fed at a single circumferential location. An example of a multiple-entry casing impingement manifold is the E^3 engine architecture shown in Figure 3.

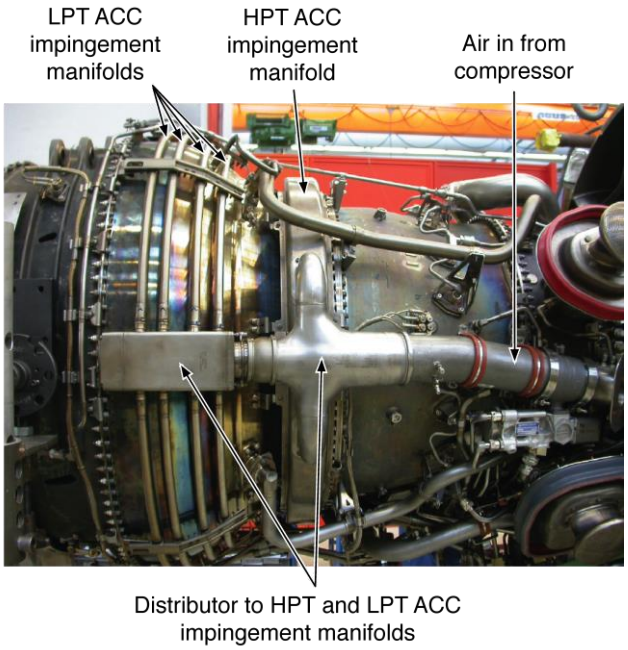

Figure 1. An MTU aero engine ACC system, adapted from 12.

Preprints (www.preprints.org) | NOT PEER-REVIEWED | Posted: 1 February 2021 doi:10.20944/preprints202102.0010.v1

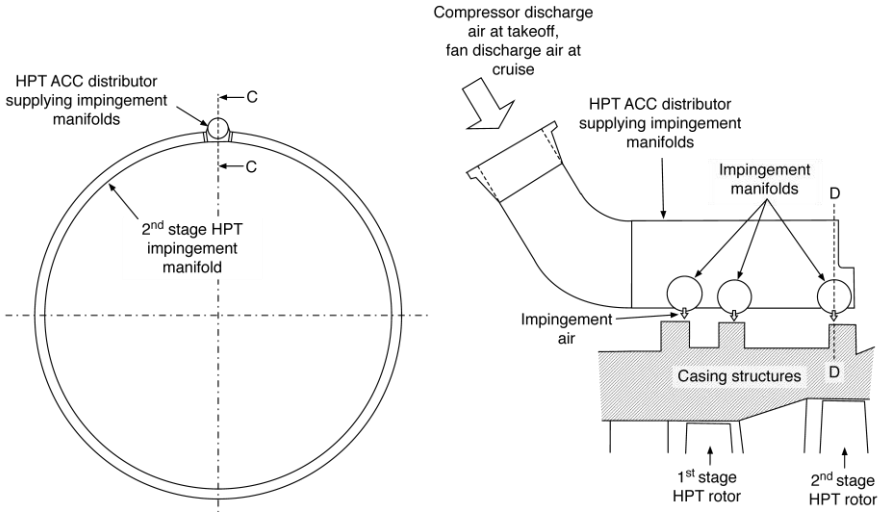

Figure 2. (a) Axial plane through the HPT ACC system of the GE CF6-6 engine. Figure adapted from 4. Position of axial plane is shown in (b) (D-D). **(b)** Meridional plane through HPT ACC system of the GE CF6-6 engine. Figure adapted from 4. Position of meridional plane is shown in (a) (C-C).

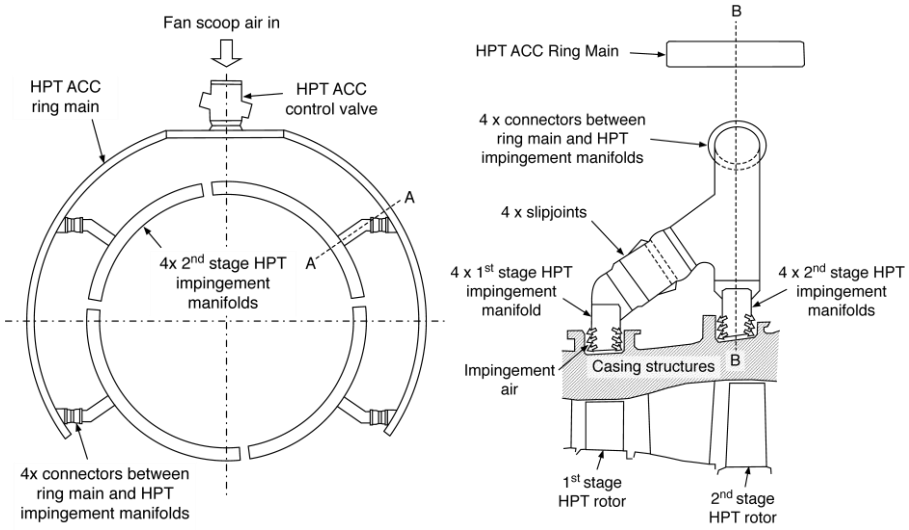

Figure 3. (a) Axial plane through the HPT ACC system developed as part of the NASA Energy Efficient Engine (E^3) program. Figure adapted from 9. Position of axial plane is shown in (b) (B-B). **(b)** Meridional plane through the HPT ACC system developed as part of the NASA Energy Efficient Engine (E^3) program. Figure adapted from 9. Position of meridional plane is shown in (a) (A-A).

While the driving design philosophy of the single-entry system is simplicity, the philosophy of the multiple-entry system is greater control, i.e. feed air more uniformly over the circumference of the impingement manifold. In this paper, we examine using computational fluid dynamics (CFD) the relative performance of the single-entry system vs the multiple-entry system. We depart from the previous literature in that we simulate the feed system (ring main, connectors etc.) as well as the impingement manifold. The domain is fully annular. Consequently, the boundary conditions at the entry to the casing impingement manifolds are more realistic, as are the secondary flow features generated within the curved domain. The enhanced fidelity gives us the unique chance to make a fair back-to-back comparison between the single-entry and multiple-entry system.

This is a timely discussion given the rapid development of novel engine architectures by aero-engine manufacturers and the sustained efforts to reduce emissions and increase SFC and time-on-

Preprints (www.preprints.org) | NOT PEER-REVIEWED | Posted: 1 February 2021 doi:10.20944/preprints202102.0010.v1

wing. As we will show, the system for supplying the casing impingement manifold has significant implications on the overall performance of the ACC system. Almost all the performance parameters discussed previously are influenced by the choice of the feed method: magnitude and uniformity of the HTC distribution, the temperature of the impinging jet, weight, manufacturability, complexity, size, ease of optimisation. We will conclude that the single-entry system outperforms the multiple-entry system on almost all performance metrics.

2. Approach

In this paper, we investigate the effect of single-entry vs multiple-entry feed on the performance of an HPT ACC system. The aerothermal performance of the candidate systems is assessed in back-to-back CFD simulations. All geometric and operating conditions not related to the inlet system are matched between the two cases. Both the single-entry and multiple-entry systems analysed in this paper are idealised version of ACC systems in current production engines. Aerothermal performance is quantitatively assessed on the basis of the HTC distribution, driving temperature difference for heat transfer between the jet and casing wall, and total pressure loss within the HPT ACC system. The geometries, CFD setup, boundary conditions and performance metrics (data reduction) are now discussed in more detail.

2.1 Single-entry ACC system geometry

The single-entry ACC system geometry is a 180° sector of an impingement manifold, shown in Figure 4. The inlet of the impingement manifold is at -90° in the circumferential direction, and the sector end wall is at +90°. The midpoint between inlet and endwall is at 0°. This convention was used to aid in describing any symmetry/asymmetry in the flow behaviour. Section E-E shows the rectangular cross-section of the manifold, with the side walls, and the four rows of holes exhausting to the surrounding pressure of 15psi, and impinging on to the casing wall.

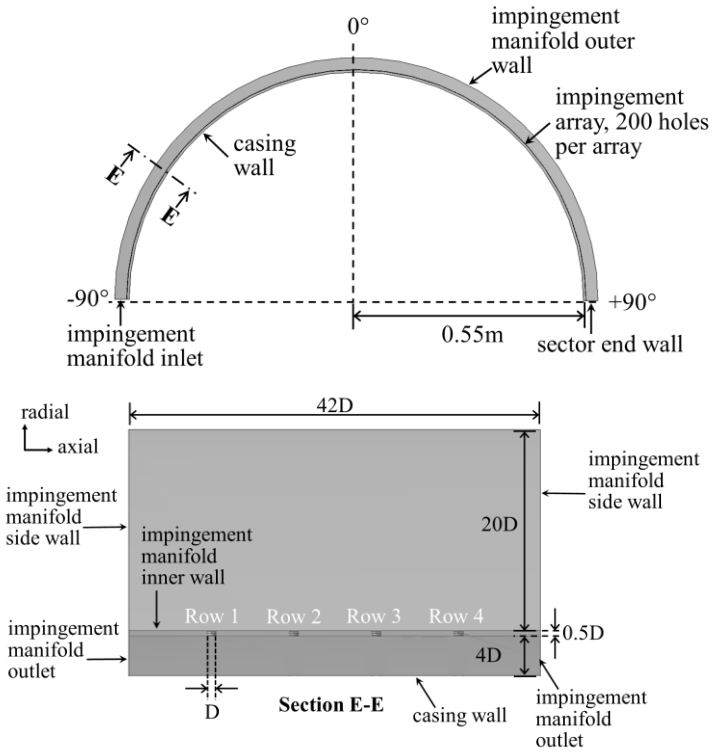

Preprints (www.preprints.org) | NOT PEER-REVIEWED | Posted: 1 February 2021 doi:10.20944/preprints202102.0010.v1

Figure 4. Single-entry ACC system geometry for CFD study.

2.2 Multiple-entry ACC system geometry

The ring main system feeds the impingement manifold system through transfer boxes at every 90°, as shown in Figure 5. Each transfer box feeds two 45° sectors of the impingement manifold. Each 45° sector of the impingement manifold has end walls, so there is no flow in between sectors. Detail F in Figure 5 shows the ring main, transfer pipe and manifold assembly, and Section G-G shows the cross-section of the assembly. The flow through the ring main exits through the ring main outlet and enters the transfer pipe. It then exits the transfer pipe and enters the impingement manifold. The impingement manifold cross-section is identical to that of the single-entry ACC system.

3. CFD Setup

The computational grid for the impingement manifold was generated in BOXERmesh 15 with 31 million nodes, with a higher density of cells centred through the impingement holes shown in Figure 6. The boundary layer along the impingement manifold inner wall was resolved with 15 prism layers. Due to the computational expense of modelling a 180° sector with 800 holes, the main passage of the manifold was kept relatively coarse. Similarly, the casing surface was resolved with 12 boundary layers, with the area in between each hole kept relatively coarse. Each of the 800 holes was resolved with 20 cells across the diameter width D, but no prism layers.

The ring main system with the transfer boxes was meshed in ANSYS Mesher, with 113,440 nodes of hexahedral elements, shown in Figure 7. The ring main system was then combined with the same impingement manifold mesh as the single entry case in the ANSYS CFX solver. Radiation was neglected in this study. The case was modelled using the steady-state RANS approximation within the ANSYS CFX solver. The k-ω SST turbulence model was used due to its versatility and robustness.

Preprints (www.preprints.org) | NOT PEER-REVIEWED | Posted: 1 February 2021 doi:10.20944/preprints202102.0010.v1

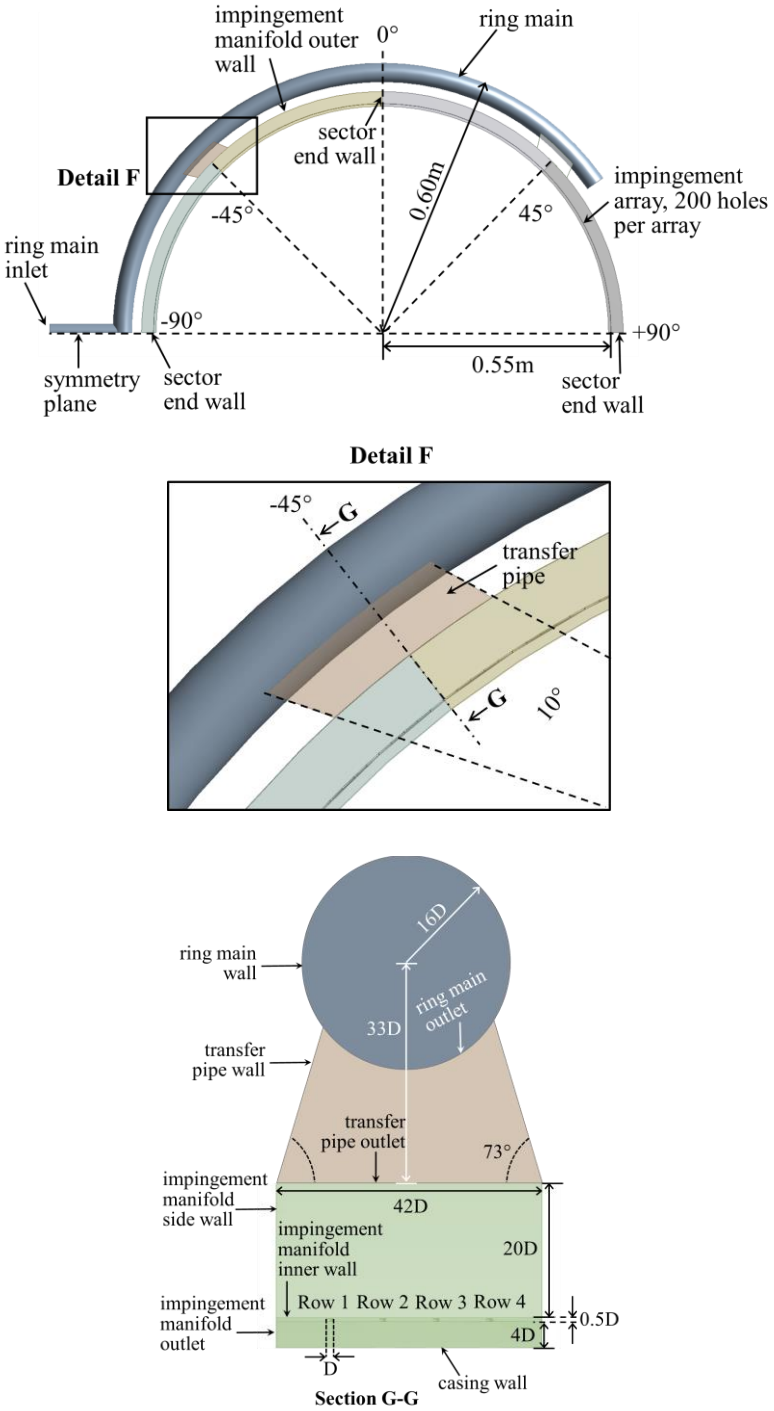

Figure 5. Multiple-entry ACC system geometry for CFD study.

In order to compare the two designs, we consider three operating conditions, based on the maximum mass flow rate delivered to the impingement system at aircraft take-off, referred to as max. takeoff. The three conditions for each of the designs are 100% of max. takeoff, followed by 50% and 20%. The details of the boundary conditions for each surface in both designs are provided in Table 1.

Preprints (www.preprints.org) | NOT PEER-REVIEWED | Posted: 1 February 2021 doi:10.20944/preprints202102.0010.v1

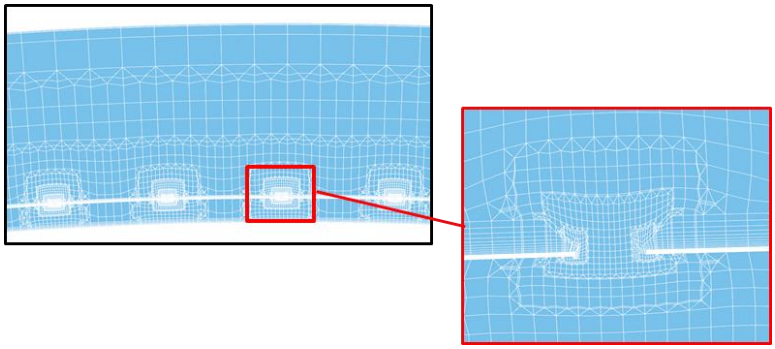

Figure 6. Cross-sectional view of computational grid for impingement manifold channel along circumferential direction using BOXERmesh, with close-up of impingement hole.

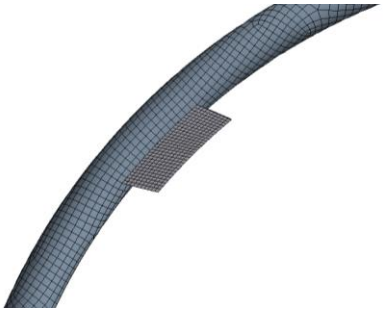

Figure 7. Computational grid for ring main and transfer box using ANSYS Mesher.

Table 1. CFD boundary conditions for both geometries

Surface	**Geometry**	**Boundary Type**	**Boundary Condition(s)**
Impingement manifold inlet	Single entry	Inlet	$\dot{m}$ = 0.2352 kg/s at 100% of max. takeoff, T = 330 K. flow direction perpendicular to surface
Impingement manifold outlet	Single entry, multiple entry	Opening	p_{static} = 15 psi, $T_{opening}$ = 600 K
Impingement manifold side wall	Single entry, multiple entry	Wall	HTC= 80 W/m²-K, $T_{outside}$ = 600 K
Impingement manifold outer wall	Single entry, multiple entry	Wall	HTC= 80 W/m²-K, $T_{outside}$ = 600 K
Impingement manifold inner wall	Single entry, multiple entry	Wall	Adiabatic
Casing wall	Single entry, multiple entry	Wall	T_{wall} = 600 K
Impingement hole walls	Single entry, multiple entry	Wall	Adiabatic
Sector end wall	Single entry, multiple entry	Wall	Adiabatic

Preprints (www.preprints.org) | NOT PEER-REVIEWED | Posted: 1 February 2021 doi:10.20944/preprints202102.0010.v1

Ring main inlet	Multiple entry	Inlet	$\dot{m}$ = 0.2352 kg/s at 100% of max. takeoff, inlet flow perpendicular to surface
Transfer pipe outlet	Multiple entry	Opening	Conservative interface flux
Transfer pipe walls	Multiple entry	Wall	Adiabatic
Ring main wall	Multiple entry	Wall	Adiabatic

4. Data Reduction

Using CFD, we quantify the heat transfer coefficient (HTC) distribution and the total pressure loss coefficient (C_{p0}) for each design, among other parameters. We consider HTC and C_{p0} the most appropriate metrics for aerothermal performance assessment since flow rate, inlet temperature and wall/gas properties are the same in each case. Symmetricity and speed of response of the tip clearance control system is indicated by the HTC distribution and engine efficiency impact of the tip clearance system is indicated by C_{p0}. The total pressure loss coefficient has been characterised by the difference in the total pressure through each hole and the total pressure at the inlet to the feed, compared to the average of the two variables (Equation (1)). In order to highlight the difference in engine efficiency impact, the multiple-entry cases have been benchmarked against the average of the hole total pressure and inlet pressure of the single-entry cases, i.e. the denominator of C_{p0} is always from a single-entry case, denoted by the subscript SE.

$$C_{p0} = \frac{(p_{0,hole} - p_{0,inlet})}{1/2(p_{0,hole} + p_{0,inlet})_{SE}} \quad (1)$$

In this case, the temperature is of less importance, since the optimum system is adiabatic to the manifold and should be targeted, although increased heat transfer to the fluid is beneficial, but comes at a penalty to the engine efficiency.

5. Results

The total pressure loss coefficient of the single-entry system is three times lower than the multiple-entry system. The multiple-entry system contains additional loss-generating mechanisms: frictional losses within the ring main and mixing/bend losses within the transfer boxes. As a consequence, the driving pressure ratio across each impingement hole in the multiple-entry system is less than in the single-entry system, for the same overall boundary conditions and impingement geometry. The individual hole (jet) Reynolds number is 1.2 times greater on average in the single-entry vs multiple-entry system impingement array, which is the primary reason why the average heat transfer coefficient on the outer-side of the turbine casing is 77% greater in the single-entry system, and 108% greater at the 30° circumferential direction, as shown in Figure 8.

The circumferential aero-thermal fields vary more smoothly in the single-entry system than the multiple-entry system. In the multiple-entry system, the aero-field in the vicinity of the transfer boxes is highly non-uniform due to the abrupt S or U bend from ring main into casing manifold, resulting in large, local circumferential variations in impingement hole mass flow rate compared to the single-entry system. The locations of the transfer boxes are visible in Figure 8 at -45° and +45°.

Preprints (www.preprints.org) | NOT PEER-REVIEWED | Posted: 1 February 2021 doi:10.20944/preprints202102.0010.v1

In contrast, the axial aero-thermal field gradients (i.e.,row to row) are lower in the multiple-entry system than in the single-entry system. The sectorised annulus and U or S bends in the multiple-entry system prevents the formation of fully-developed counter-rotating secondary flow vortices by reducing the available smooth development length, limiting axial HTC variation. The secondary flow vortices are clearly seen in the single-fed system after an initial entry length, as shown in Figure 9. This gives flow preference to the two inner impingement rows which generate 26% more HTC than the two outer impingement rows, with the differences more pronounced at the four peaks at -65°, -35°, +25° and +75°. These peaks represent the onset of the secondary flow vortices as the flow moves around each 45° bend in the 180° sector. The vortices are set up by the centrifugal and pressure forces acting on the faster moving core flow and causing an adverse pressure gradient 16. The effect is less prominent in the two outer rows. Nevertheless, all impingement rows in the single-entry system generate greater HTCs than the impingement rows in the multiple-entry system for the 100% massflow rate condition.

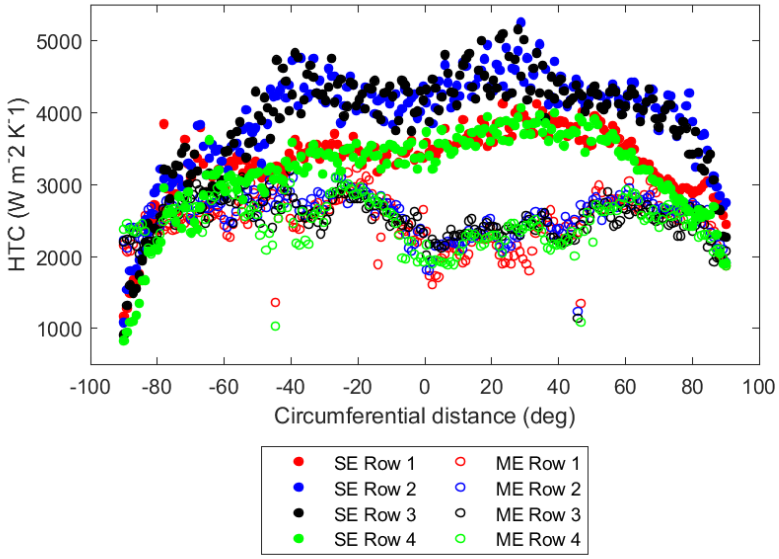

Figure 8. Circumferential distribution of local peak HTC on casing surface across each all four arrays of holes for both single-entry (SE) and multiple-entry (ME) cases at 100% massflow rate condition.

Preprints (www.preprints.org) | NOT PEER-REVIEWED | Posted: 1 February 2021 doi:10.20944/preprints202102.0010.v1

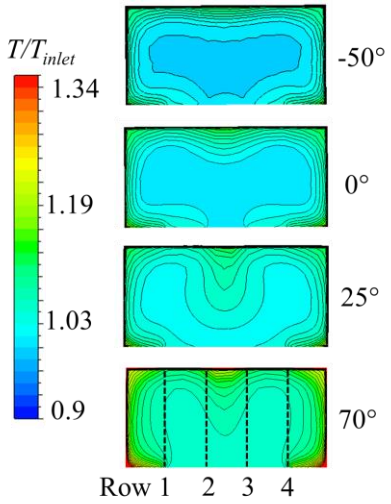

Figure 9. Cross-sectional temperature profiles for single-entry case at 100% massflow rate condition, at four circumferential positions showing development of secondary flow vortices.

The low values of HTC for the single-entry case in the circumferential region between -90° to -70° are caused by the flow separation within the hole due to the adverse turning angle and higher manifold channel mass velocity (G_c). This means that the flow is not perpendicular to the impingement manifold inner wall as it exits through the hole, as seen in Figure 10, and has a lower hole discharge coefficient of 0.58. The flow close to +90° has a higher hole discharge coefficient because of the lower channel mass velocity to jet mass velocity ratio, i.e. lower G_c/G_j. This highlights a scope for design optimisation of the single-entry system in this region.

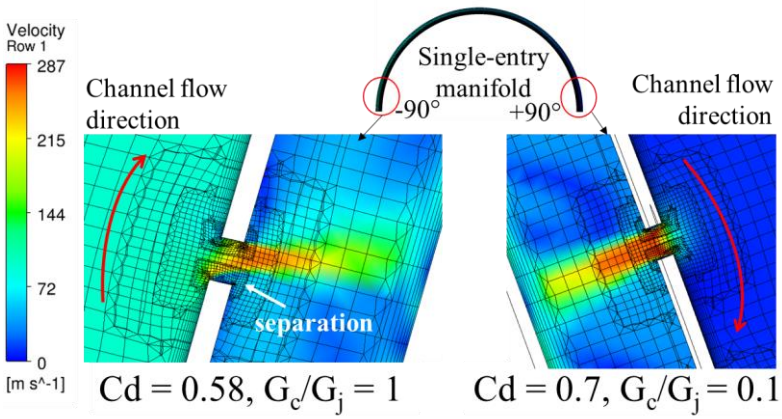

Figure 10. Cross-section of aero-field through Row 1 holes near -90° and +90° for single-entry case.

The 50% and 20% massflow rate conditions show similar trends for the HTCs in Figure 11 and Figure 12, however, the levels are lower due to the reduced massflow rates. For the single-entry case, there are now three peaks instead of four, suggesting that the Reynolds number of the manifold channel affects the formation of the secondary flow features. The HTC delivered by the multiple-entry system is similar in value to the single-entry system between -90° and -20°, while the sector from 0° to 45° sees a large drop in HTC values. This is likely due to this sector being upstream of the 45°- 90° sector, but is fed by the same transfer box. Hence, the flow exiting the 45°-transfer box not only has decreased

Preprints (www.preprints.org) | NOT PEER-REVIEWED | Posted: 1 February 2021 doi:10.20944/preprints202102.0010.v1

total pressure due to frictional losses in the ring main, but now has to work against the forward momentum to deliver massflow to the upstream sector.

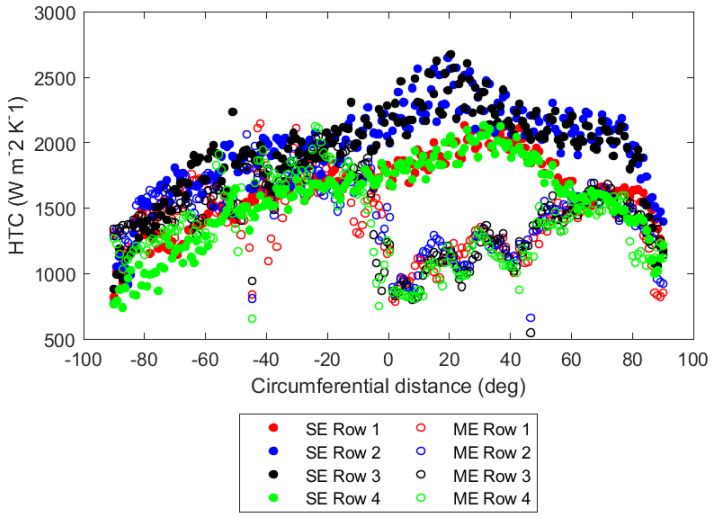

Figure 11. Circumferential distribution of local peak HTC on casing surface across each all four arrays of holes for both single-entry and multiple-entry cases at 50% massflow rate condition.

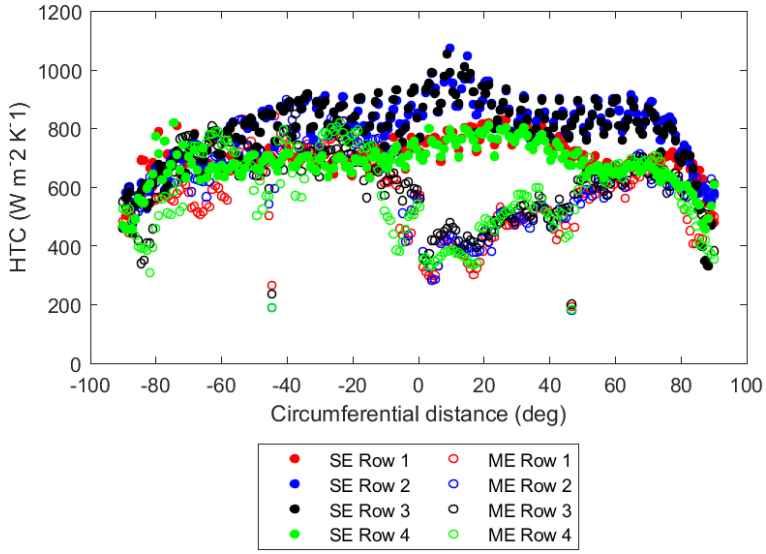

Figure 12. Circumferential distribution of local peak HTC on casing surface across each all four arrays of holes for both single-entry and multiple-entry cases at 20% massflow rate condition.

Preprints (www.preprints.org) | NOT PEER-REVIEWED | Posted: 1 February 2021 doi:10.20944/preprints202102.0010.v1

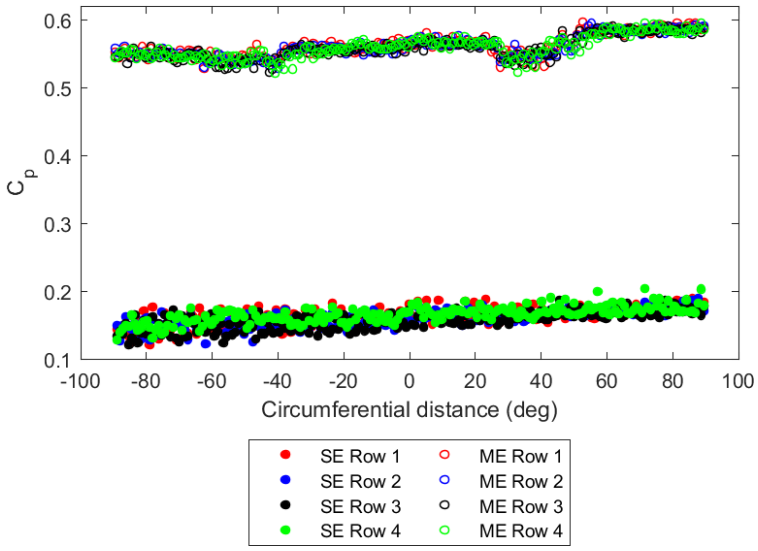

Figure 13. Circumferential distribution of C_P across all four arrays of holes for both single-entry and multiple-entry cases at 100% massflow rate condition.

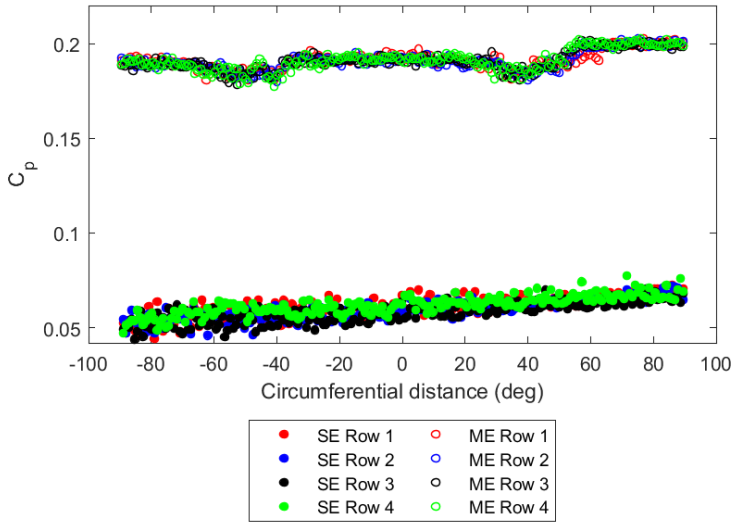

Figure 14. Circumferential distribution of Cp across all four arrays of holes for both single-entry and multiple-entry cases at 50% massflow rate condition.

Preprints (www.preprints.org) | NOT PEER-REVIEWED | Posted: 1 February 2021 doi:10.20944/preprints202102.0010.v1

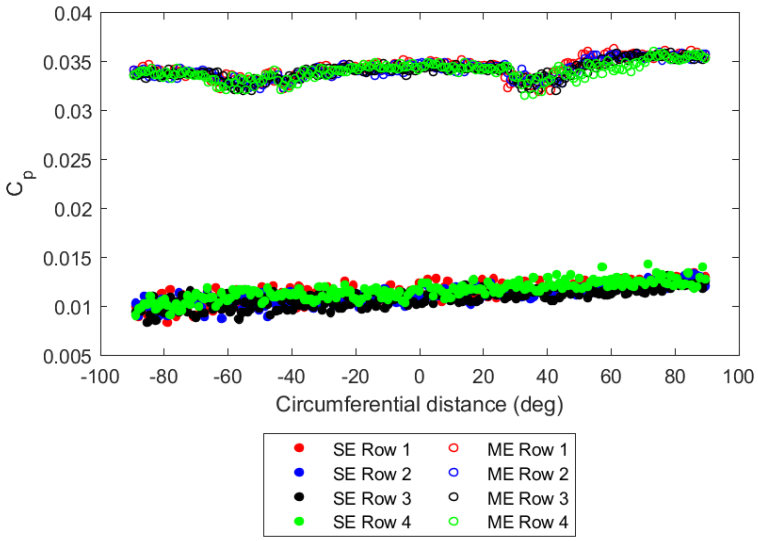

Figure 15. Circumferential distribution of Cp across all four arrays of holes for both single-entry and multiple-entry cases at 20% massflow rate condition.

Figures Figure **13**-Figure **15** show the circumferential distribution of the total pressure loss coefficient $\boldsymbol{C_{p0}}$ for the same three massflow rate cases discussed previously. The coefficient has been normalised to that of the average of the hole total pressure and inlet total pressure for the single-entry case (Equation 1). In

Figure 13, the average $\boldsymbol{C_{p0}}$ for the multiple-entry case is three times higher compared to the single-entry case. This indicates that the multiple-entry system sees a higher total pressure loss, therefore requires a higher driving pressure ratio. The gradient for the single-entry system increases by 39% and for the multiple-entry system by 7.5%. The multiple-entry system experiences larger circumferential non-uniformities in the aero-field, compared to the relatively smooth, linear increase in the single-entry system. The advantage of the lower circumferential total pressure loss is lost due to the overall higher values of total pressure loss and lower HTCs.

In Figure 14, the values of $\boldsymbol{C_{p0}}$ are lower for the 50% massflow rate condition, as expected. The trend in the circumferential gradient is also similar to that of the 100% massflow are cases. The multiple-entry case continues to see a total pressure loss that is three times higher than that of the single-entry system. The 20% massflow rate condition in Figure 15 shows that this remains true for a lower driving pressure ratio as well.

Of interest to ACC system designers is also the circumferential increase in temperature of the coolant air, which can reduce the convective heat transfer by 20% and increase the amount of circumferential asymmetry17. Figures Figure **16** - Figure **18** reiterate the conclusions from the previous discussion. In Figure 16, comparing the temperature rise between the jet temperature and inlet temperature shows that the multiple entry experiences an increase of up to 40° temperature across both 45° sectors, while the single entry case ranges from 5° to 20 °. The single entry case experiences a drastic increase towards the closed end of the manifold at +90° as the flow velocity drastically reduces. Both designs perform

Preprints (www.preprints.org) | NOT PEER-REVIEWED | Posted: 1 February 2021 doi:10.20944/preprints202102.0010.v1

worse with respect to temperature rise and asymmetry as the massflow rate is reduced, as shown in Figure 17 and Figure **18**.

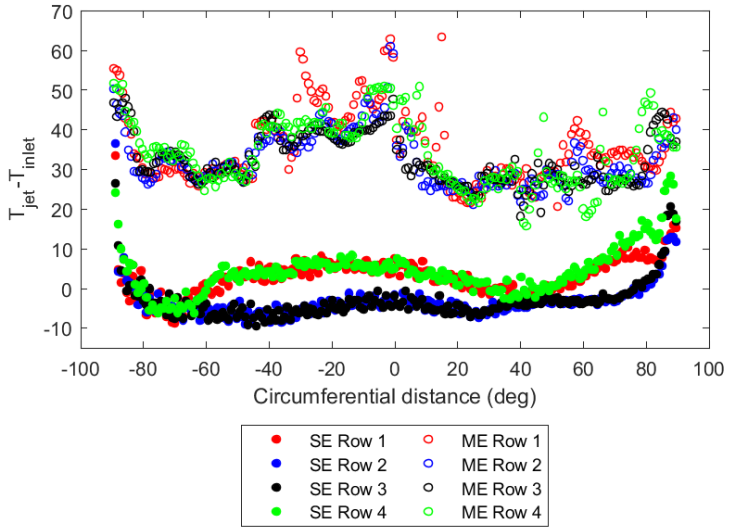

Figure 16. Circumferential distribution of increase in temperature across all four arrays of holes for both single-entry and multiple-entry cases at 100% massflow rate condition.

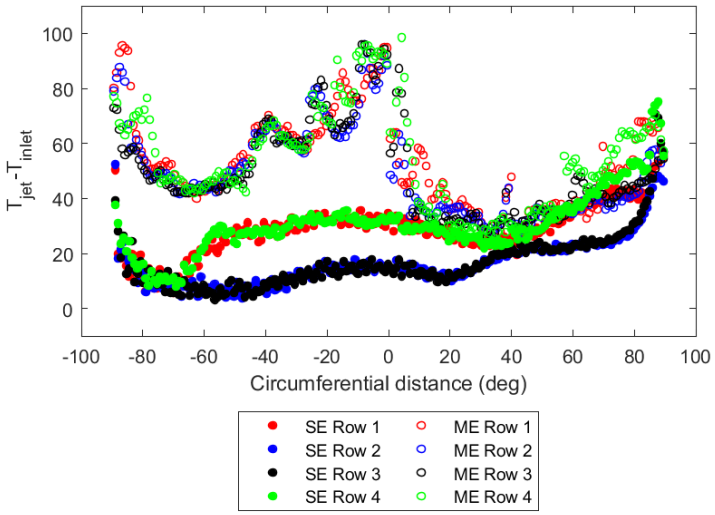

Figure 17. Circumferential distribution of increase in temperature across all four arrays of holes for both single-entry and multiple-entry cases at 50% massflow rate condition.

Preprints (www.preprints.org) | NOT PEER-REVIEWED | Posted: 1 February 2021 doi:10.20944/preprints202102.0010.v1

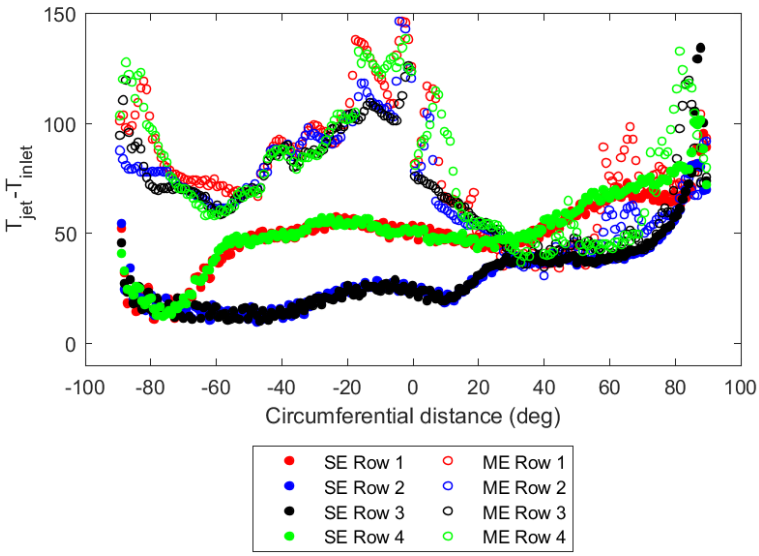

Figure 18. Circumferential distribution of increase in temperature across all four arrays of holes for both single-entry and multiple-entry cases at 20% massflow rate condition.

6. Conclusions

In this paper we compare using CFD the aerothermal performance of two candidate casing manifolds for supplying an impingement-actuated active tip clearance control system for an aero-engine HP turbine. The two geometries are (a) *single-entry*: an annular manifold fed at one circumferential location; (b) *multiple-entry*: a casing manifold split into four annular sectors, each sector supplied separately from an annular ring main.

From the results of this computational study, and in consideration of holistic aero-engine design factors, we conclude that a single-entry system is closer to an optimal solution than a multiple-entry system. The reasons are summarised as follows.

6.1 Engine efficiency

All else being equal, a single-entry system requires less overall driving pressure ratio than a multiple-entry system to provide the same heat transfer performance, since the total pressure loss coefficient is less and the average HTC is greater in the single-entry system. In order for the multiple-entry system to generate the same HTC as the single-entry system, it must operate at a higher overall system pressure ratio in order to achieve the same mass flow rate and jet Reynolds number. Subsequently the manifold system must be supplied from a higher pressure stage of the compressor, reducing engine efficiency.

6.2 Response time

The single-entry system transfers heat faster than the multiple-entry system for the same overall pressure ratio, since the HTC (convective heat transfer) and mass flow rate (advective heat transfer) are greater in the single-entry system. Therefore, the active tip clearance system responds faster in the single-entry system, with a corresponding increase in engine efficiency. Seen from another perspective, the multiple-entry system would require a greater overall pressure ratio than the single-

Preprints (www.preprints.org) | NOT PEER-REVIEWED | Posted: 1 February 2021 doi:10.20944/preprints202102.0010.v1

entry system to achieve the same speed of response (HTC), which is less efficient for the reasons described previously.

6.3 Ease of optimisation

The systems presented in this paper are early iterations of production casing manifold systems. An important consideration when down-selecting the manifold supply system is the ease with which the designs may subsequently be optimised, to maximise HTC field uniformity on the casing and to minimise flow requirement. In this respect, aero-thermal fields that are smooth with small gradients and deterministic flow features are a distinct advantage.

The aero-thermal fields in the single-entry system have much smoother, smaller gradients than those in the multiple-entry system. While the counter-rotating vortices in this iteration of single-entry system generate non-uniform HTC in the axial direction, they do so in a way that is consistent and well-understood. The axial HTC non-uniformity may easily be remedied, for example by increasing the hole sizes of the outermost impingement rows. Similarly, the circumferential HTC distribution in the single-entry system is predictable, based on reliable discharge coefficients, blowing ratios and pressure drop. Circumferential HTC may, for example, be optimised by varying the cross-sectional area of the manifold with circumference or varying the spacing/diameter of the holes. In theory, optimisation of the single-entry system could be achieved through hand-calculation.

There are large, local aero-thermal field variations in the multiple-entry system, and these are highly sensitive to the flow and geometric boundary conditions. Any optimisation must then occur at a very fine level to capture the local variation, and it is likely that hole spacing and diameters will vary discretely, rather than varying smoothly and continuously as in the single-entry system. This necessitates a more computationally expensive optimisation method, e.g. CFD coupled with geometry optimisation schemes. Even after optimisation, a multiple-entry system will be highly sensitive to uncertainties in boundary conditions, numerical errors, and fluid approximations because of the steep aero-thermal field gradients.

6.4 Weight, Cost and Complexity

Clearly, the weight of the single-entry system is less than the weight of the multiple-entry system, because the multiple-entry system incorporates a ring main and transfer boxes. Not only does this affect the power-to-weight ratio of the engine, it also increases complexity and cost of design, manufacture, operation and maintenance.

The next stage in the engine development process is design optimisation. While the manifold designs presented in this paper are by no means local maxima in performance, this study provides strong evidence that the global optimum for tip clearance casing manifold design is far nearer a single-entry system, than a multiple-entry system. Although, the issues encountered by the multiple-entry system may help inform future design scenarios where a controlled circumferential non-uniformity in HTC is sought to correct asymmetric clearance. This would require multiple valves and/or an iteration of the ring main-transfer box assembly design considered in this study.

Acknowledgements: The support of Rolls-Royce plc is gratefully acknowledged.

 doi:10.20944/preprints202102.0010.v1

Nomenclature

Abbreviations

ACARE	Advisory Council of Aeronautic Research in Europe
ACC	Active clearance control
CFD	Computational fluid dynamics
HPT	High-pressure turbine
HTC	Heat transfer coefficient
SE	Single-entry
ME	Multiple Entry
SFC	Specific fuel consumption

Variables

C_{p0}	Total pressure loss coefficient $\frac{(p_{0,hole}-p_{0,inlet})}{1/2(p_{0,hole}+p_{0,inlet})_{SE}}$
G_c	Channel mass velocity (velocity x density)
G_j	Jet mass velocity (velocity x density)

References

1. Wilfert, G., Sieber, J., Rolt, A., Baker, N., Touyeras, A. and Colantuoni, S., 2007, "New environmental friendly aero engine core concepts," in XVII International Symposium of Air Breathing Engines, Beijing, pp. 2-7, Paper No. ISABE-2007-1120.
2. Denton, J.D., 1993, "Loss Mechanisms in Turbomachines," ASME J. Turbomach., 115(4), pp.621-656.
3. Lattime, S.B., Steinetz, B.M. and Robbie, M.G., 2002, "Turbine Engine Clearance Control Systems: Current Practices and Future Directions," NASA/TM 2002-211794.
4. Rich, S.E. and Fasching, W.A., 1982, "CF6 Jet Engine Performance Improvement - High Pressure Turbine Active Clearance Control," NASA CR-165556.
5. Wiseman, M.W. and Guo, T-H., 2001, "An Investigation of Life Extending Control Techniques for Gas Turbine Engines," Proceedings of the American Control Conference, Arlington, VA.
6. Ruiz, R., Albers, B., Sak, W., Seitzer, B. and Steinetz, B., 2006, "Benefits of Improved HP Turbine Active Clearance Control," NASA Seal/Secondary Air System Workshop.
7. Howard, W.D. and Fasching, W.A., 1982, "CF6 Jet Engine Diagnostics Program; High Pressure Turbine Roundness/Clearance Investigation," NASA CR-165581.
8. Dann, A., Dhopade, P., Bacic, M., Ireland, P. and Lewis, L., 2017, "Experimental and Numerical Investigation of Annular Casing Impingement Arrays for Faster Casing Response," ASME J. Eng. Gas Turbines Power, 139(9).
9. Halila, E.E., Lenahan, D.T. and Thomas, T.T., 1982, "Energy efficient engine high pressure turbine test hardware detailed design report," NASA CR-167955.
10. Choi, M., Gillespie, D.R.H. and Lewis, L.V., 2018, "The Effect of External Casing Impingement Cooling Manifold Standoff Distance on Casing Contraction for Thermal Control of Blade Tip Clearance," ASME J. Turbomach., 140(2).

11. Choi, M., Dyrda, D.M., Gillespie, D.R.H., Tapanlis, O. and Lewis, L.V., 2016, "The Relative Performance of External Casing Impingement Cooling Arrangements for Thermal Control of Blade Tip Clearance," ASME J.Turbomach., 138(3).
12. Ben Ahmed, F., Tucholke, R., Weigand, B. and Meier, K., 2011, "Numerical Investigation of Heat Transfer and Pressure Drop Characteristics for Different Hole Geometries of a Turbine Casing Impingement Cooling System," ASME Paper No. GT2011-45251.
13. Mao, J., Yao, T., Han, X., He, Z. and He, K., 2018, "Numerical study of the radiation effect on the jet array impinging heat transfer in a feeding pipe," Numerical Heat Transfer, Part A: Applications, 73(2), pp.125-142.
14. Dann, A.G., Thorpe, S.J., Lewis, L.V. and Ireland, P., 2014, "Innovate measurement techniques for a cooled turbine casing operating at engine representative thermal conditions," ASME Paper No. GT2014-26092.
15. Dawes, W., Harvey, S., Fellows, S., Eccles, N., Jaeggi, D. and Kellar, W., 2009, "A Practical Demonstration of Scalable, Parallel Mesh Generation," 47th AIAA Aerospace Sciences Meeting including The New Horizons Forum and Aerospace Exposition.
16. Miller, Donald S. BHRA Association. 1978, "Internal flow systems." Cranfield, Bedfordshire.
17. Da Soghe, R., Bianchini, C., 2019, "Aero-Thermal Investigation of Convective and Radiative Heat Transfer on Active Clearance Control Manifolds," ASME Paper No. GT2019-90007.